Soft Matter

PAPER

Cite this: *Soft Matter*, 2016, **12**, 4093

Influence of the structure on the collapse of poly(*N*-isopropylacrylamide)-based microgels: an insight by quantitative dielectric analysis

Man Yang and Kongshuang Zhao*

Received 31st December 2015,
Accepted 16th March 2016

DOI: 10.1039/c5sm03155a

www.rsc.org/softmatter

The collapse of poly(*N*-isopropylacrylamide)/poly(acrylic acid) semi-interpenetrating polymer network (PNIPAM/PAA SIPN) and poly(*N*-isopropylacrylamide-*co*-acrylic acid) (P(NIPAM-*co*-AA)) microgel suspensions is studied by dielectric spectroscopy in a frequency range from 40 Hz to 110 MHz as a function of temperature. Dielectric measurements show that the structure affects the relaxation behavior of microgels: two relaxations (micro-Brownian motion and interfacial polarization at low frequency and counterion polarization at high frequency) are observed in the SIPN microgel whose charges mainly exist in domains and one relaxation (interfacial polarization) is observed in the copolymer microgel whose charges distribute in the whole network. A dielectric model is proposed to describe the collapsed microgel suspensions, from which some parameters, such as the volume fraction and the permittivity of microgels, were calculated using Hanai's equation. The temperature dependencies of these parameters show that the SIPN microgel has better low-temperature swelling properties and thermal responsiveness. This is caused by different polymer-solvent and electrostatic repulsion interactions in different microgels. Compared with pure PNIPAM, the relationship of volume phase transition temperature (VPTT) is $VPTT_{P(NIPAM\text{-}co\text{-}AA)} > VPTT_{PNIPAM/PAA\ SIPN} > VPTT_{PNIPAM}$, and it is explained from the viewpoint of interaction. Besides, the activation energy data prove that the structure influences the electrical properties of microgels, which is consistent with the results obtained from quantitative dielectric analysis.

1. Introduction

Poly(*N*-isopropylacrylamide) (PNIPAM), a typical temperature-sensitive gel, can be fabricated as an interpenetrating/semi-interpenetrating polymer network (IPN/SIPN) or a copolymer, depending on the doping substances and methods. The thermally induced collapse transition of these polymer microgels in aqueous liquids has been investigated extensively because it is closely related to protein denaturation and other biological phenomena.[1,2] Besides, the collapse transition of PNIPAM-based microgels is also a key problem that is involved in many applications such as biomedicine[3] and catalysis,[4] which is determined mainly by the thermal collapse behavior. Therefore, relevant fundamental problems, such as the influence of the structure and ionic monomer distribution of microgels on their volume phase transition (VPT), have become one of the important issues in polymer physics.

In general, incorporation of ionic monomers into the PNIPAM network not only increases the volume phase transition temperature, but also subtly influences the mechanism of VPT.[5–7] For neutral hydrogels their dimensions under equilibrium conditions are determined by the elasticity of the polymer network and the osmotic pressure, and incorporating ionic monomers into the gel network can accommodate an additional osmotic contribution to the swelling of microgels. However, the case of the (S)IPN microgel that has two relatively independent networks is different from that of the copolymer microgel that has only one single network. The two networks in the (S)IPN microgel are actually phase-separated from the microscopic view and the second network will form domains in the first network.[8,9] Therefore, the interaction between the polymer and solvent in the (S)IPN microgel is obviously different from that in copolymer microgels. This leads to a different volume phase transition behavior between the two systems. In copolymer microgels, the ionic monomers were randomly distributed in the network. It has been found that charged groups will increase the swelling ratio[6] and volume phase transition temperature (VPTT)[10] of microgels. Kratz *et al.*[11] also observed a two-step volume transition process with the increase of ionic monomers. If the amount of ionic monomers is considerable, the thermal responsiveness of copolymer microgels may decrease and even disappear.[12] For the (S)IPN microgel, Kozhunova[13]and Zhang[14] found that the charged chains or networks will affect the VPTT of IPN microgels,

College of Chemistry, Beijing Normal University, Beijing, 100875, China. E-mail: zhaoks@bnu.edu.cn

while Stile[15] and Zhou[16] draw an opposite conclusion. We[15] studied the PNIPAM/PAA SIPN microgel and found that the doped PAA chains affect the microstructure, thermal responsiveness and VPTT of the SIPN microgel. The above studies show that although the volume phase transition behavior of SIPN and copolymer microgels has been reported by many researchers, the effects of ionic monomers and doped polymers on the collapse of PNIPAM-based microgels are still under debate, and especially, few studies made a comparison between these two microgels with different structures. A comparison study on the collapse process of copolymers and S(IPN) microgels is necessary because it enables us to examine the conformation and interaction of microgels that have different structures during the collapse process, and also helps us to understand the relevance between the macroscopic phase behavior and the microscopic structure of microgels.

Most of the characterization methods used to study the VPT of microgels are infrared spectroscopy, electron microscopy, and light scattering and so on, which give information on the molecular structure and size of microgels during the volume phase transition process. Alternatively, dielectric spectroscopy is a sensitive tool to detect the structure and electrical properties of different systems, especially heterogeneous systems.[16] Some researchers have used this method to study the collapse transition of microgels with different structures. For example, Fullbrandt[17] monitored the VPT of PNIPAM microgels with different cross-linking density by both the frequency and temperature dependence of the conductivity spectra, and obtained information on the internal structure of the microgels. Zhou *et al.*[18] characterized PNIPAM microgels with different charge distribution and cross-linking density distribution by DLS and dielectric spectroscopy. In a recent dielectric study on PNIPAM microgels that have different distributions of cross-linking density, we revealed that the spatial distribution of the cross-linking density almost does not influence the VPTT, but significantly affects their swelling capacity at low temperature.[19] Besides, we[15] also compared the thermal responsiveness of PNIPAM/PAA SIPN microgels with different contents of PAA by quantitative dielectric analysis. The above research proves that dielectric spectroscopy is an effective tool to probe the microstructures of different microgels and two recent studies by us[15,19] also show that the quantitative dielectric modeling analysis, which can give information on the volume fraction, water content, and electrical parameters of microgels, has advantages in detecting the collapse transition.

In the present work, two PNIPAM-based microgels with different structures, *i.e.*, PNIPAM/PAA SIPN and P(NIPAM-*co*-AA), were studied. The structural characteristics of these two microgels are given in Fig. 1. For the microgel with semi-interpenetrating network structure, although interpenetration can be realized by controlling the preparation process, the two networks are actually phase-separated from the microscopic view:[8,9,20] linear PAA forms a domain in the PNIPAM network. For the P(NIPAM-*co*-AA) microgel, the monomers AA are randomly bonded to the network. Because the charges are introduced by PAA and AA, *i.e.*, the charged groups of the SIPN microgel are mainly in the domains formed by PAA, and those of the copolymer microgel are dispersed in the entire network as shown in Fig. 1. Based on their different dielectric behaviors, we discussed the difference of their collapse process by quantitative dielectric modeling analysis, and explained the difference from the view of electrostatic interaction.

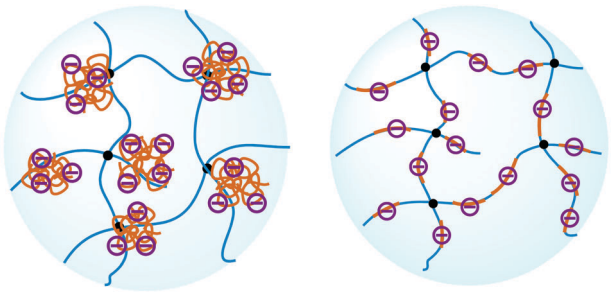

(a) PNIPAM/PAA SIPN microgel (b) P(NIPAM-*co*-AA) microgel

Fig. 1 Schematic diagram of the microgel with different structures: (a) PNIPAM/PAA SIPN and (b) P(NIPAM-*co*-AA). The blue line is the PNIPAM network, and the brown line is PAA. ⊖ represents negative charge.

2. Experimental section

2.1 Preparation of microgels

Materials. *N*-Isopropylacrylamide (NIPAM) was provided by Tokyo Chemical Industrial Co., Ltd and recrystallized with *n*-hexane, then stored in brown bottles at 4 °C. *N*,*N*,*N*′*N*′-Tetramethylethylene-diamine (TEMED), acrylic acid (AA), and *N*,*N*′-methylene-bisacrylamide (MBA) as a crosslinker were purchased from Sinopharm Chemical Regent Beijing Co., Ltd Span 80 was bought from Farco Chemical supplies, Beijing, China. Ammonium persulfate (APS) as an initiator was supplied from Shantou Xilong Chemical Factory Guangdong, China. Sodiumhydroxide, sulfuric acid and cyclohexane were bought from Beijing Chemical Works, China. All these reagents were of analytical grade and used as received. Deionized water used throughout the preparation process was produced by RiOs-water system (Millipore Corp., America).

Preparation. The PNIPAM/PAA SIPN, P(NIPAM-*co*-AA) and PNIPAM microgels with an average size of 6.0 ± 1.4 μm were prepared using a premix membrane emulsification technique as already reported elsewhere.[21–23] For the preparation of PNIPAM/PAA microgels, typically, NIPAM and the linear PAA chains with a crosslinking agent MBA and an initiator APS were commingled together with water as the aqueous phase. Cyclohexane containing a certain amount of Span 80 was used as the oil phase. The prepared coarse emulsion by mixing the oil phase and water with low speed stirring was extruded through the SPG membrane under a certain nitrogen pressure to get the final emulsion. Then, TEMED dissolved in cyclohexane was added into the emulsion to initiate the polymerization at 25 °C. After 4 h, the obtained microspheres were centrifuged and washed with acetone and water. The obtained microspheres were dispersed in deionized water for further use.

P(NIPAM-*co*-AA) and PNIPAM microgels were obtained following the same method as used for the preparation of PNIPAM/PAA SIPN microgels. The mass fraction of the AA monomer in both PNIPAM/PAA and P(NIPAM-*co*-AA) microgels is 20%. The only difference was that AA monomers instead of linear PAA chains were added in the water phase in the preparation of P(NIPAM-*co*-AA) microgels, and AA monomers were absent in the water phase in the preparation of PNIPAM microgels. Because APS was introduced in the preparation process and the pH value of the three microgel suspensions used for dielectric measurement was around 5.34, the counter-ion in microgel suspensions was mainly NH_4^+.

2.2 Dielectric measurements and analysis

Dielectric measurements of microgel suspensions were carried out over a frequency range of 40 Hz to 110 MHz using 4294A Impedance Analyzers (Agilent Technologies). The temperature range of the measurements was between 25 °C and 55 °C. A dielectric measuring cell with concentrically cylindrical platinum electrodes (the effective area of the electrodes was 78.5 mm^2 and the electrode distance was 8 mm) was employed. The temperature of the samples was controlled using a circulating thermostatic water jacket. The raw data, capacitance C_x and conductance G_x, were corrected by the cell constant C_l and residual inductance L_r (arising from terminal leads) based on the following eqn (1) and (2) according to Schwan's method.[24] The stray capacitance C_r (3.17 nF) and the cell constant C_1 (0.456 pF) are determined by using three standard substances (air, ethanol and pure water) according to the relation $C_j = \varepsilon_j C_l + C_r$ (ε_j and C_j are the permittivity and the measured capacitance of the standard substances). The value of L_r (11.1 nH) is determined by plotting C_i against G_i^2 (C_i and G_i denote the measured capacitance and conductance of KCl solutions with different concentrations at lower frequencies respectively) according to Schwan's lumped circuit method.[24]

$$C_s = \frac{C_x\left(1+\omega^2 L_r C_x\right)+L_r G_x^2}{\left(1+\omega^2 L_r C_x\right)^2+\left(\omega L_r G_x\right)^2} - C_r \quad (1)$$

$$G_s = \frac{G_x}{\left(1+\omega^2 L_r C_x\right)^2+\left(\omega L_r G_x\right)^2} \quad (2)$$

where ω (=$2\pi f$; f is the measurement frequency of the applied ac field) is the angular frequency.

Then the permittivity and conductivity of the microgel suspensions were obtained by taking into account the relationship of $\varepsilon = C_s/C_l$ and $\kappa = G_s\varepsilon_0/C_l$ (where $\varepsilon_0 = 8.8541 \times 10^{-12}$ F m^{-1} is the vacuum permittivity). The complex permittivity is expressed as

$$\varepsilon^*(\omega) = \varepsilon(\omega) - j\varepsilon''(\omega) = \varepsilon(\omega) - j\frac{\kappa(\omega)-\kappa_l}{\omega\varepsilon_0} \quad (3)$$

where ε^* is the complex permittivity and ε'' is the dielectric loss. ω is the angular frequency and $j = (-1)^{1/2}$. κ_l is the low-frequency limit of conductivity, which was read out from the conductivity spectroscopy at low frequency. For the solution or suspension with higher ionic strength, like this case, the electrode polarization (EP) effect, due to large capacitive impedance at electrode surfaces adjacent to an electrolyte solution, will cover the low-frequency relaxation at least partly and the dielectric data at low frequency cannot be analyzed accurately. To eliminate the electrode polarization effect, some methods such as the logarithmic derivative method[25] and the conductivity analysis method[26] have been developed. In this work, we use a relatively simple method to remove electrode polarization, *i.e.*, fitting permittivity with Cole–Cole eqn (4)[27] containing the EP term $A\omega^{-m}$ (where A and m are adjustable parameters). It is clearly seen that although electrode polarization is relatively large, especially for the SIPN microgel system (Fig. 2(a)), the relaxation at lower frequencies can be recovered after the contribution of EP was subtracted from the raw permittivity data by A and m.

$$\varepsilon^* = \varepsilon_h + \sum_g \frac{\Delta\varepsilon_g}{1+\left(j\omega\tau_g\right)^{\beta_g}} + A\omega^{-m} \quad (4)$$

where ε_h is the high-frequency limit of permittivity, $\Delta\varepsilon_g$ and τ_g (=$1/(2\pi f_{0g})$, f_{0g} is characteristic relaxation frequency) indicate the

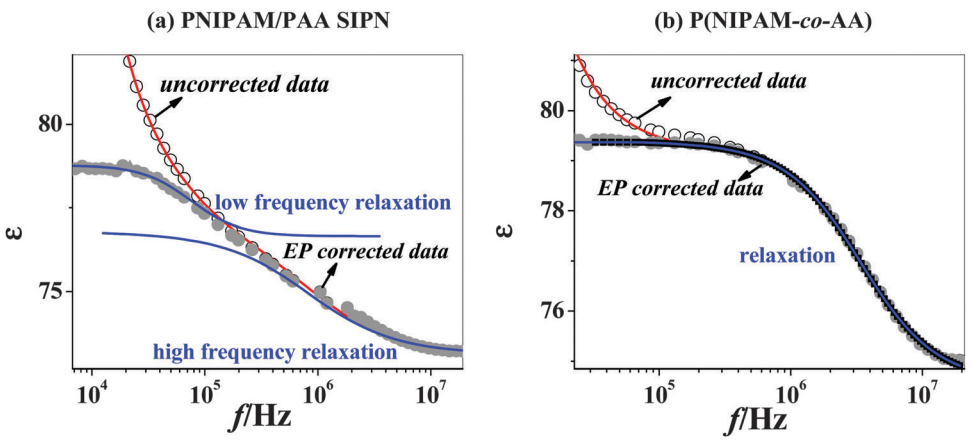

Fig. 2 Permittivity of (a) PNIPAM/PAA SIPN and (b) P(NIPAM-*co*-AA) microgel suspensions at 30 °C. The hollow and solid circles are the uncorrected raw data and corrected curves after subtraction of the EP effect respectively. The fitted uncorrected raw data and the relaxations are represented by red and blue solid lines respectively.

relaxation strength and relaxation time of the gth relaxation, respectively; $\beta_g (0 < \beta_g \leq 1)$ is the Cole–Cole parameter.

Furthermore, the new dielectric data (*i.e.*, the corrected permittivity data without EP) obtained were fitted by using eqn (4) without $A\omega^{-m}$. The curve-fitting was carried out using the Levenberg–Marquard method to minimize the sum of the residuals for the real part and imaginary part of complex permittivity.

$$\chi = \sum_i \left[\varepsilon_e'(\omega_i) - \varepsilon_t'(\omega_i)\right]^2 + \sum_i \left[\varepsilon_e''(\omega_i) - \varepsilon_t''(\omega_i)\right]^2 \quad (5)$$

where the subscripts e and t are the experimental and theoretical values, respectively, and ω_i is the ith angular frequency. Because of large errors in the imaginary part, only the real part of eqn (4) was fitted to experimental data to minimize the following residual

$$\chi = \sum_i \left[\varepsilon_e'(\omega_i) - \varepsilon_t'(\omega_i)\right]^2 \quad (6)$$

As a representative case, the dielectric spectra of SIPN and P(NIPAM-*co*-AA) microgel suspensions at 30 °C are shown in Fig. 2. The hollow circles represent the permittivity without EP, and the solid line represents the best fitting curve using eqn (4) with two and one Cole–Cole terms for PNIPAM/PAA SIPN and P(NIPAM-*co*-AA) respectively. As can be seen in Fig. 2, the dielectric spectra of the PNIPAM/PAA SIPN microgel and the P(NIPAM-*co*-AA) microgel were all well represented with the best-fit dielectric relaxation parameters.

3. Results and discussion

Although the electrode polarization (EP) is relatively large and covers part of the relaxation, the Cole–Cole equation (without EP) including two relaxations gave a best-fit curve (see the solid circle curves after eliminating the EP effect) as shown in Fig. 2(a). This fitting result shows that two dielectric relaxation processes at around 10^5 and 10^6 Hz occur in these SIPN microgel systems, which were also confirmed by our previous work,[15] while only one relaxation can be found for the copolymer P(NIPAM-*co*-AA) microgel at 10^6–10^7 Hz. Besides, we have also measured the dielectric behavior of electrically neutral PNIPAM microgels under the same conditions, and no relaxation was observed. From the above analysis, we draw a preliminary conclusion that the number of relaxations is related to the charge or structure of microgels.

Fig. 3 shows three-dimensional representations of the dielectric spectra corrected according to the method described in Section 2.2 for the three microgel suspensions (PNIPAM, PNIPAM/PAA, and P(NIPAM-*co*-AA)). The black solid lines are the ε–f curves below, around and above the volume phase transition temperature, respectively. It is clear that the frequency dependence of the corrected permittivity change significantly as the temperature increases. The temperature dependences of the corrected permittivity at certain frequency (blue solid lines) show that the permittivity of PNIPAM microgel suspension $\varepsilon_{\text{PNIPAM}}$ at lower frequency (below 10^5 Hz) decreases suddenly at around 34 °C; while $\varepsilon_{\text{PNIPAM/PAA}}$ increases to a peak at 36 °C and then decreases (Fig. 3(b)); and the slower decline of $\varepsilon_{\text{P(NIPAM-}co\text{-AA)}}$ is accelerated significantly at 38 °C. The difference in the temperature dependence of permittivity among the three systems will be interpreted later in Fig. 9. To further obtain the information on the microscopic mechanisms of the collapse transition process of the different microgels from the dielectric parameters, we fitted the dielectric spectra of PNIPAM/PAA SIPN and P(NIPAM-*co*-AA) microgel suspensions shown in Fig. 3 using the method described in Section 2.2 and the best-fit relaxation parameters (strength of dielectric relaxation $\Delta\varepsilon$, relaxation time τ) obtained are listed in Table 1.

3.1 Relaxation mechanism: influence of the structure on the relaxation behavior

Fig. 4 shows the temperature dependence of relaxation strength $\Delta\varepsilon$ for two different structural microgel suspensions. As temperature increases, $\Delta\varepsilon_{\text{SIPN}}$ of low frequency relaxation appears as a peak at about 36 °C; $\Delta\varepsilon_{\text{SIPN}}$ of high frequency relaxation decreases slowly and further decreases suddenly at about 36 °C; $\Delta\varepsilon_{\text{P(NIPAM-}co\text{-AA)}}$ decreases gradually with temperature over the temperature ranges but has a slight turning point at around 38 °C. The different turning points of the above two microgel

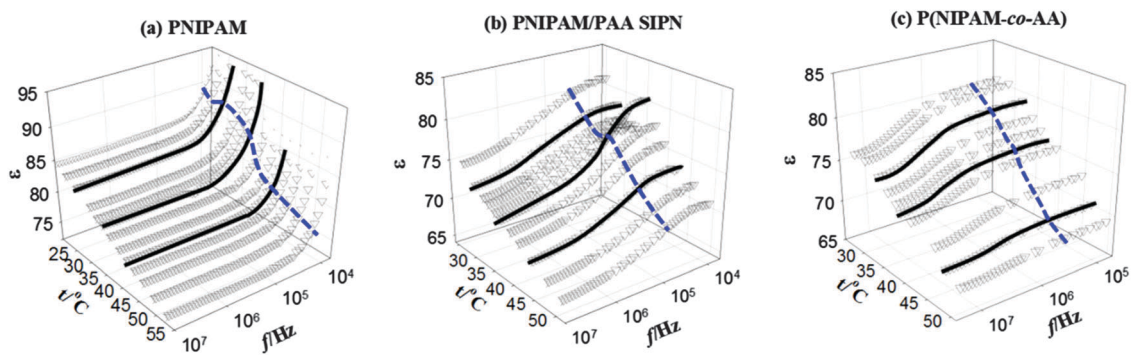

Fig. 3 The permittivity *versus* frequency and temperature in three-dimensional representations for: (a) PNIPAM, (b) PNIPAM/PAA SIPN (corrected data), and (c) P(NIPAM-*co*-AA) microgel (corrected data). The black solid lines are the ε–f curves below, around and above the transition temperature. The blue dotted lines are the ε–t curves under certain frequency.

Table 1 Relaxation parameters of PNIPAM/PAA SIPN (a) and P(NIPAM-*co*-AA) (b) microgel suspensions at various temperatures

(a)

t/°C	$\Delta\varepsilon_1$	$\Delta\varepsilon_h$	τ_l/μs	τ_h/μs
27.2	3.22 ± 0.18	3.61 ± 0.22	2.05 ± 0.12	0.37 ± 0.04
30.0	2.21 ± 0.14	3.73 ± 0.18	1.87 ± 0.09	0.39 ± 0.03
32.2	2.22 ± 0.24	3.22 ± 0.25	1.67 ± 0.08	0.36 ± 0.02
33.5	2.13 ± 0.28	3.31 ± 0.28	1.63 ± 0.08	0.30 ± 0.02
35.0	2.84 ± 0.16	3.34 ± 0.16	1.68 ± 0.08	0.30 ± 0.01
36.4	7.40 ± 0.20	3.44 ± 0.20	3.05 ± 0.14	0.33 ± 0.02
39.0	6.41 ± 0.20	1.60 ± 0.20	1.82 ± 0.08	0.73 ± 0.04
41.0	6.10 ± 0.18	1.21 ± 0.15	1.75 ± 0.09	0.66 ± 0.05
44.0	4.92 ± 0.16	1.00 ± 0.16	1.43 ± 0.07	0.64 ± 0.04
47.6	4.00 ± 0.18	0.92 ± 0.18	1.16 ± 0.06	0.64 ± 0.03
50.8	3.51 ± 0.18	0.84 ± 0.22	1.07 ± 0.05	0.58 ± 0.03

(b)

t/°C	$\Delta\varepsilon$	τ/ns
27.2	5.21 ± 0.27	48.6 ± 2.3
29.9	4.92 ± 0.22	46.7 ± 2.3
33.0	4.51 ± 0.30	42.8 ± 1.9
35.2	4.23 ± 0.28	40.5 ± 2.0
37.0	3.91 ± 0.16	38.3 ± 1.2
38.0	3.81 ± 0.17	38.1 ± 1.2
40.3	3.00 ± 0.16	37.6 ± 1.3
45.5	1.73 ± 0.18	48.0 ± 1.8
47.6	1.44 ± 0.19	57.6 ± 2.3
50.5	1.13 ± 0.20	68.9 ± 2.2

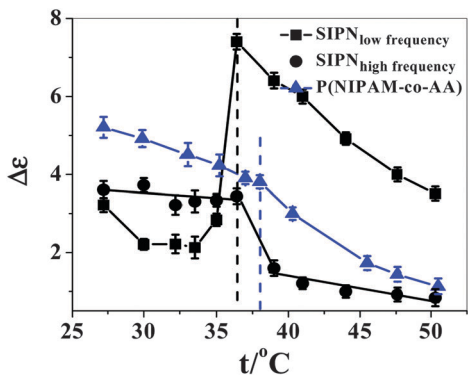

Fig. 4 Temperature dependence of the dielectric strength of different microgels.

systems indicate that they have different VPTTs. This strongly indicates that the VPTT of microgels is related to their structure. In order to understand the possible microscopic mechanisms of the collapse process and structural changes before and after the collapse, the present microgel suspension systems are modeled as particle dispersion as illustrated in Fig. 5 showing that the swollen microgels collapse into compact microspheres (taking the copolymer microgel as an example). This is convenient for discussion, especially for the subsequent dielectric analysis.

3.1.1 Relaxation mechanism of the PNIPAM/PAA SIPN microgel. For particle dispersion, in general two dielectric relaxations caused by counterion polarization and interfacial polarization, respectively, occur in radio frequency areas. Counterion polarization is from the tangential and radial migration of counterion along the particle;[28,29] interfacial polarization is from the accumulation of charge at the interface of two phases with different electrical properties.[16] According to the theories developed by Shilov[30,31] and often used by Grosse[28] and Delgado[29] to describe the low relaxation of suspensions, the relaxation frequency f_0 related to the counterion polarization is proportional to the counterion diffusion coefficient counterion of D and inversely to the square of particle radius r:

$$\tau = 2\pi f_0 \sim D/r^2 \quad (7)$$

Substituting the size[15] of the SIPN microgel (6 μm) and that of the PAA domain (50 nm) into eqn (7), respectively, using the diffusion coefficient of NH_4^+ (1.957×10^{-5} cm^2 s^{-1} at 25 °C), the relaxation time for the counterion polarization of the SIPN microgel is estimated to be around 3–8 ms (20–60 Hz), while that of the PAA domain is estimated to be around 0.32 μs (0.5 MHz). The relaxation time for the counterion polarization of the PAA domain is close to the characteristic time of the high frequency relaxation of the SIPN microgel as listed in Table 1a. Therefore, we confirm that the high frequency relaxation is caused by the tangential and radial diffusion of counterions around the charged PAA domain.[15]

The low frequency relaxation of the PNIPAM/PAA SIPN microgel is attributed to the micro-Brownian motion of side groups in PNIPAM above VPTT and interface polarization above VPTT, as has been confirmed by our previous work.[15,19] Below VPTT, the SIPN microgel is in a highly swollen state, and the hydrogen bonds between the amide groups and water molecules are not favourable to the micro-Brownian motion of the PNIPAM segment, resulting in a relatively low contribution of dielectric increment $\Delta\varepsilon_{SIPN}$ to the low frequency relaxation (black square in Fig. 4). As temperature rises, part of the hydrogen bonds between amide and water molecules are broken, leading to the speeding up of random orientation of side groups of PNIPAM. Therefore, $\Delta\varepsilon_{SIPN}$ increases and relaxation time τ_{SIPN} decreases with temperature as listed in Table 1a. When the temperature is increased above VPTT, the hydrogen bonds between amide groups and water broke further and the intramolecular hydrogen bond formed between the amide groups of PNIPAM molecules as illustrated in Fig. 8(a).[32] Thus the micro-Brownian of PNIPAM segment is not favored and both the dielectric parameters ($\Delta\varepsilon_{SIPN}$ and τ_{SIPN} (Table 1a)) of the low frequency relaxation begin to decrease. Because the microgel loses water and collapses into a compact microsphere above VPTT, the interface between microgel particles and water medium becomes relatively clear as illustrated in Fig. 5. Therefore, the low-frequency relaxation above VPTT is contributed by interfacial polarization.[15]

3.1.2 Relaxation mechanism of P(NIPAM-*co*-AA) microgels. In the case of the copolymer microgel P(NIPAM-*co*-AA), the only relaxation located at around 10^6–10^7 Hz is not from counterion polarization, because this relaxation should appear at 3–8 ms (20–60 Hz) in the microgel with a size of 6 μm as analyzed above. The interfacial polarization is the main reason for the current relaxation. According to the interfacial polarization model of suspension,[33] the counterion migration distance

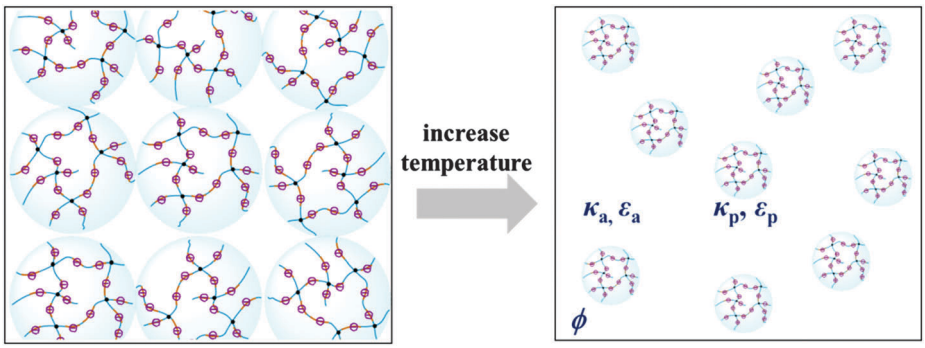

Fig. 5 Schematic diagram of microgel suspension during volume phase transition by taking the copolymer microgel as a representative case. ε_a, κ_a are the permittivity and conductivity of the water phase, respectively. ε_p, κ_p and ϕ denote the permittivity, conductivity and volume fraction of the collapsed microgel particles.

can be characterized by the Debye length χ^{-1}, which is equivalent to the thickness of the EDL surrounding the microsphere. The time necessary for the counterion to migrate the distance χ^{-1}, which is equivalent to relaxation time τ_χ, is determined using the following equations:[33]

$$\tau_\chi = \chi^{-2}/D \tag{8}$$

$$\chi^{-1} = \sqrt{\frac{\varepsilon_a \varepsilon_0 KT}{e^2 \sum_i C_i Z_i^2}} \tag{9}$$

$$\varepsilon_a = 0.24921 \times 10^3 - 0.79069 \times T + 0.72997 \times 10^{-3} \times T \tag{10}$$

where D is the diffusion coefficient of the counterion, C and Z are the concentration and valence of the ion, respectively, ε_a is the permittivity of continuous medium in the suspension. By substituting $D_{NH_4^+}$ at each temperature[34] and experimental relaxation time τ_χ into eqn (8), the obtained χ^{-1} varies between 10–15 nm. The fluctuation is much smaller than the microgel diameter. Meanwhile, χ^{-1} reduces as temperature increases and is in accordance with the change trend of eqn (9). This proves that the relaxation above VPTT is caused by interfacial polarization.

3.1.3 Influence of the network structure. By analyzing the relaxation mechanisms of different microgels it is revealed that their relaxation behavior is closely related to their structures. Firstly, interfacial polarization exists in the charged PNIPAM/PAA SIPN and charged P(NIPAM-*co*-AA) microgels, while not in the uncharged PNIPAM. This is because both the PNIPAM/PAA SIPN and P(NIPAM-*co*-AA) microgels have the electrical properties that evidently differ from the medium.[35] This indicates that the introduced charged groups significantly affect the dielectric properties of microgels. Secondly, the SIPN microgel also shows an additional micro-Brownian motion. For copolymer microgels, the monomer NIPAM can form hydrogen bonds with the adjacent monomer AA, thus, the motion of NIPAM will be limited by the carboxyl group; while for the SIPN microgel, the PAA chains are mainly in the domains shown in Fig. 1 and hardly interact with NIPAM. As a result, the movement of the side chain of PNIPAM will not be restricted. Therefore, the SIPN microgel shows an additional motion mode of macromolecules. The above analysis indicates that network structure influences the relaxation behavior, electrical properties and chain movement of microgels.

3.2 Influence of the structure on the collapse behavior of microgels

The collapsed SIPN and copolymer microgel solution can be described as a particle suspension: the microgel microspheres with permittivity ε_p and conductivity κ_p are dispersed in a continuous aqueous medium of ε_a and κ_a in volume fraction ϕ as illustrated in Fig. 5. The complex permittivity ε^* of the suspension is given by Hanai's equation[16]

$$\frac{\varepsilon^* - \varepsilon_p^*}{\varepsilon_a^* - \varepsilon_p^*}\left(\frac{\varepsilon_a^*}{\varepsilon^*}\right)^{1/3} = 1 - \phi \tag{11}$$

where ε_p^* and ε_a^* are the complex permittivity of the microspheres and the medium, respectively. The parameters (ε_p, ε_w, κ_p, κ_w, ϕ) characterizing the electrical properties of the suspension (described in the dielectric model of Fig. 5 and here called phase parameters) are numerically calculated using Hanai's equation[16] described in literature studies.[19,36–38] The phase parameters calculated are shown in Table 2.

These parameters, especially the permittivity of collapsed microgel ε_p and volume fraction ϕ, change significantly below and above VPTT. To study the thermal responsiveness of microgels, we define C as the collapse parameter, which is a measure of the collapse degree of the microgel using the following equation:

$$C = \frac{\phi_0 - \phi_t}{\phi_0} \tag{12}$$

where ϕ_0 and ϕ_t are the volume fraction of the microgel at initial temperature and t °C, respectively. Fig. 6(a) shows the temperature dependence of the collapse parameter C. Obviously, C increases sharply for the PNIPAM/PAA SIPN microgel and P(NIPAM-*co*-AA) copolymer microgel, respectively, at different temperatures (shadows with different colors), suggesting that collapse transition occurs at different temperatures for the two different microgels. Moreover, C_{SIPN} of the SIPN microgel is

Table 2 Phase parameters of PNIPAM/PAA SIPN and P(NIPAM-*co*-AA) copolymer microgel suspensions at different temperatures

t/°C	ϕ	κ_a (mS m^{-1})	κ_p (mS m^{-1})	ε_p
(a)				
27.2	0.64	0.98	1.90	76.3
30.0	0.64	1.10	1.92	74.7
32.2	0.60	1.18	2.02	75.2
33.5	0.56	1.23	2.09	74.7
35.0	0.58	1.18	2.16	74.1
36.4	0.39	1.16	3.02	73.1
39.0	0.38	1.32	3.14	67.0
41.0	0.35	1.44	3.22	63.4
44.0	0.32	1.54	3.41	62.4
47.6	0.31	1.63	3.29	61.2
50.8	0.29	1.74	3.27	59.2
(b)				
27.2	0.65	0.39	0.80	74.9
29.9	0.64	0.41	0.82	73.8
33.0	0.62	0.46	0.87	72.4
35.2	0.64	0.47	0.88	71.7
37.0	0.61	0.50	0.91	70.6
38.0	0.64	0.49	0.90	70.7
40.3	0.43	0.61	1.00	67.7
45.5	0.39	0.70	1.00	65.5
47.6	0.37	0.75	1.01	63.9
50.5	0.36	0.80	1.03	63.0

Notes: the data at $T <$ VPTT are only for reference, because in this temperature range it is inappropriate to explain the swollen microgel solution using interface polarization theory.

larger than the $C_{copolymer}$ of the copolymer, which implies that the SIPN microgel has better thermal responsiveness.

The collapse transition process can also be seen in Fig. 6(b) in which the temperature dependence of the permittivity of the microgels shows a inflexion at about 36 °C for PNIPAM/PAA SIPN microgels and 38 °C for P(NIPAM-*co*-AA) copolymer microgels. It is generally known that the apparent permittivity of microgels can be expressed as,[36]

$$\varepsilon_p = \varepsilon_w f_w + \varepsilon_{polymer}(1 - f_w) \quad (13)$$

where ε_w and $\varepsilon_{polymer}$ are the permittivity of pure water and the polymer matrix, respectively; f_w is the water content in the microgel. The decrease of ε_p as the temperature increases means that the water molecules within the microgels are expelled out continuously and the microgels collapse. The abrupt decrease of ε_p implies that the volume phase transition occurs, and the turning points indicate the volume phase transition temperature VPTT.

The water content f_w in microgels calculated from eqn (13) (take $\varepsilon_{polymer}$ as an approximate value of 5) can directly describe the collapse process of microgels (Fig. 7):

(1) For the SIPN microgel, f_w is relatively larger than P(NIPAM-*co*-AA) microgels below VPTT, indicating that the SIPN microgel has better swelling properties at low temperatures. This is because both the carboxyl groups of PAA and amide groups of PNIPAM can capture water molecules through hydrogen bonding as illustrated in Fig. 8(a).[14] The larger change rate of f_w above VPTT shows that the SIPN microgel is more prone to collapse and lose water molecules. This means that the electrostatic repulsion that hinders the collapse of the PNIPAM network is weakened since most of the charges exist in domains and are relatively separated from the PNIPAM network.

(2) For P(NIPAM-*co*-AA) microgels, the value of f_w is smaller than that of the SIPN microgel below VPTT because only part of the amide bonds could capture water molecules, and the others formed intramolecular hydrogen bonds[39] with the carboxyl group at low temperature (Fig. 8(b)). In addition, when temperature is above VPTT the rate of change of f_w is slower than that of the SIPN microgel, which indicates that the fixed charges, which were directly bound to the PNIPAM network as shown in Fig. 1 and 8(b), generated strong electrostatic repulsion, as a result, the collapse transition of PNIPAM was hindered.

In short, because of the difference in the electrostatic repulsion, essentially in structure, SIPN microgels collapse more easily than copolymer microgels. As a consequence, the volume of the collapsed SIPN microgel is relatively small (high-temperature region in Fig. 6(a)), which also implies that the SIPN microgel may have higher release efficiency in drug delivery.[40]

3.3 Influence of the structure on the VPTT of microgels

Both the measured dielectric spectra and calculated phase parameters reveal that the VPTT of SIPN and copolymer microgels is different. To investigate the influence of the structure on the VPTT of different microgels, we take the permittivity of PNIPAM, PNIPAM/PAA and P(NIPAM-*co*-AA) microgel suspensions at 10 kHz,

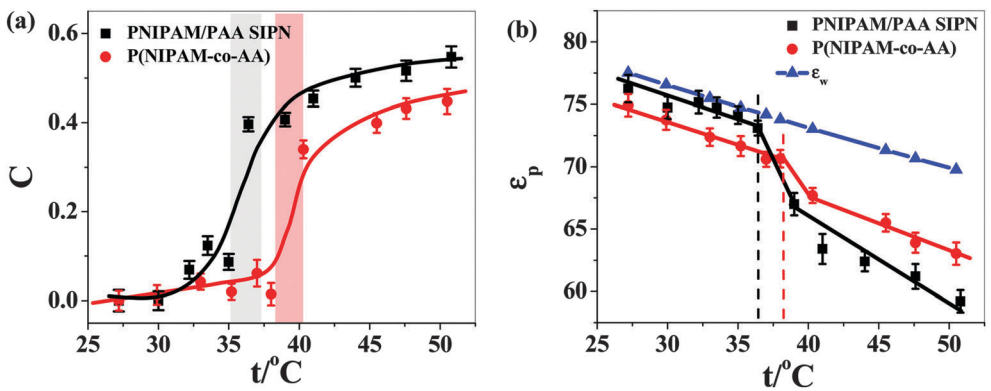

Fig. 6 Temperature dependence of the (a) collapse parameter C and (b) permittivity of microgel and water (ε_p, ε_w).

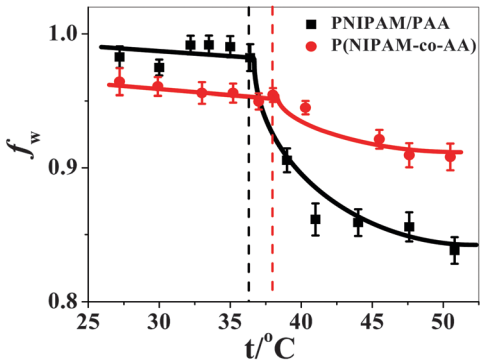

Fig. 7 Temperature dependence of the water content of PNIPAM/PAA SIPN and P(NIPAM-*co*-AA) microgels. The value below the VPTT in only for reference since it is inappropriate to explain the swollen microgel solution with interface polarization theory in this temperature range.

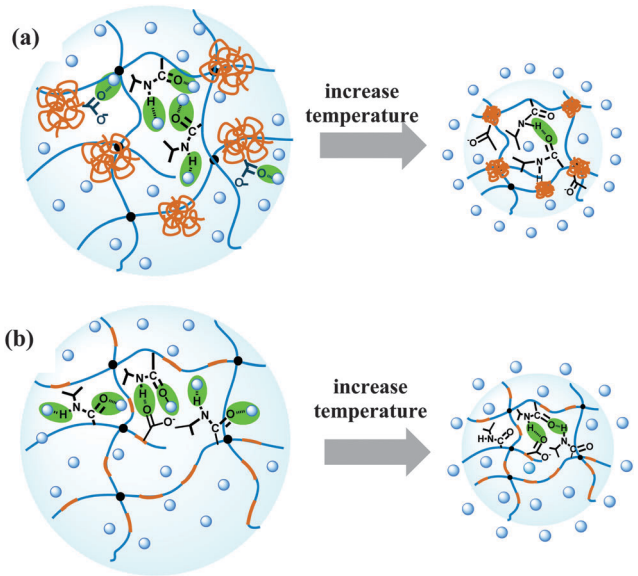

Fig. 8 The interaction of (a) SIPN microgel and (b) copolymer microgel during collapse transition.

the equivalent of their low-frequency permittivity, to plot their dependence on temperature, and the results are compared in Fig. 9. In this figure, the permittivity of different microgels decreases and turns at different temperatures (dashed lines): $VPTT_{P(NIPAM\text{-}co\text{-}AA)} > VPTT_{PNIPAM/PAA} > VPTT_{PNIPAM}$.

It is generally perceived that the phase transition behavior of the polymer is actually the result of competitive intermolecular interactions.[41] For PNIPAM microgel aqueous solution the intermolecular interaction includes: hydrogen bonding interaction of NIPAM–H_2O (facilitates dissolution) and the hydrophobic interaction of PNIPAM dependent isopropyl groups as well as that of the backbone (facilitates phase separation). Below VPTT the hydrogen bonding interaction between PNIPAM and H_2O plays a dominant role, therefore, PNIPAM microgels can swell in water at low temperatures. When temperature increases, the hydrogen bond between PNIPAM–H_2O weakens and hydrophobic interaction dominates, and this leads to the

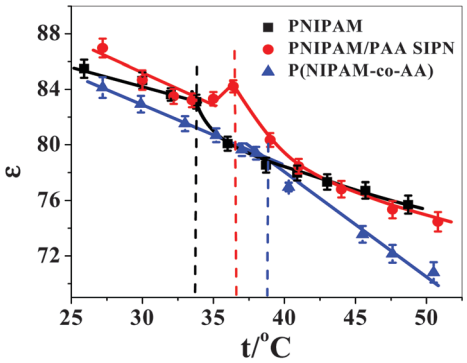

Fig. 9 Temperature dependence of permittivity for different microgel suspensions at 10 KHz.

collapse of microgels. Thus, the polymer "solvation-phase separation" can be switched by strengthening one of these interactions or by weakening another.[42] After introducing carboxyl groups to the network, typically two opposite effects will affect: on one hand, the carboxyl groups make microgels more hydrophilic, which reduces VPTT; on the other hand, the charged groups increase the internal electrostatic repulsion of the microgel network, so it needs to overcome the additional electrostatic free energy to collapse, as a result, VPTT increased.[43] From Fig. 9, it is obvious that both the VPTT of the SIPN and copolymer microgel are higher than the pure PNIPAM, suggesting that the electrostatic repulsion plays a major role in relevant interactions. For the microgel with the same amount of charges but different structures, $VPTT_{P(NIPAM\text{-}co\text{-}AA)} > VPTT_{PNIPAM/PAA}$ indicates that the electrostatic repulsion generated by the fixed charged groups in the PNIPAM network is stronger than that interpenetrated in the PNIPAM network.

3.4 Thermodynamic analysis of relaxation processes

Relaxation phenomena could be viewed as a process in which energy changes from state A to state B through a potential barrier E_a. From the temperature-dependent dielectric spectra we can obtain the relaxation rate constant k which has a reciprocal relationship with the relaxation time ($k = 1/\tau$).[44] Then, the potential barrier E_a of the relaxation processes can be obtained by the following Eyring equation[45]

$$\ln \tau = A + \frac{E_a}{RT} \quad (14)$$

where A is a constant which only varies slowly with temperature and R is the gas constant.

According to eqn (14), the plots of $\ln(\tau)$ against $1/T$ for the PNIPAM/PAA SIPN and P(NIPAM-*co*-AA) microgel systems are shown in Fig. 10. Evidently, the linear relationship between $\ln \tau$ and T is divided into two line segments around VPTT. From the intercepts of these regression lines, E_a is obtained and summarized in Table 3.

We focus on the potential barrier E_a of interfacial polarization processes (shown in boldface of Table 3). Since the interfacial polarization includes essentially the diffusion migration of counterion in EDL, the potential barrier of this relaxation

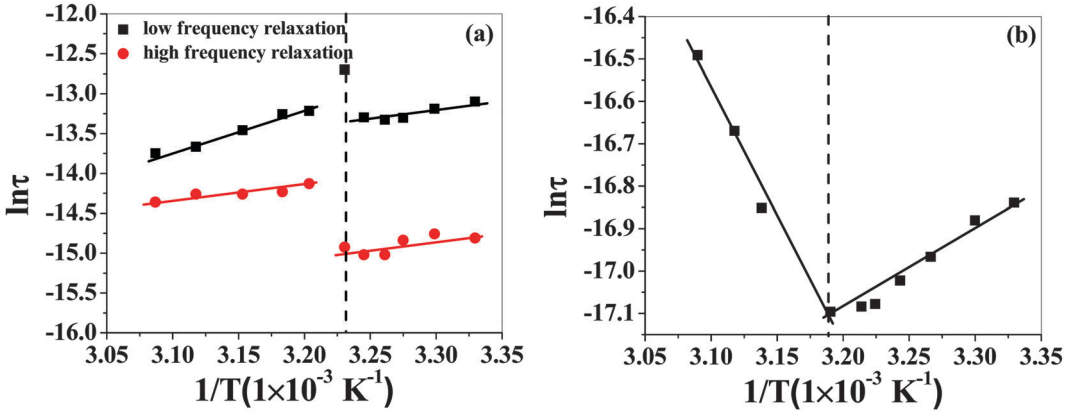

Fig. 10 Arrhenius plots of (a) SIPN and (b) copolymer microgels.

Table 3 Activation energy estimated using eqn (14) for different microgels

	PNIPAM/PAA SIPN					
	Low frequency relaxation		High frequency relaxation		P(NIPAM-*co*-AA)	
	$T <$ VPTT	$T >$ VPTT	$T <$ VPTT	$T >$ VPTT	$T <$ VPTT	$T >$ VPTT
E_a/(kJ mol^{-1})	29.2	**41.2**	25.0	13.3	−50.2	**17.2**

process depends on the electrostatic attraction from the surface charge of microgels. It can be seen that the E_a of interfacial polarization for PNIPAM/PAA SIPN microgels is smaller than that of P(NIPAM-*co*-AA) microgels. This means that the counterions of the former are easily free from fixed charges to be polarized, *i.e.*, the surface charge density of SIPN microgels may be larger than that of copolymer microgels. This result is consistent with the conductivity data of microgels in Table 2, and also indirectly proves that the electrical properties of microgels will be influenced by charge distribution (network structures essentially).

4 Conclusions

Dielectric behaviors of PNIPAM/PAA SIPN and P(NIPAM-*co*-AA) microgel suspensions were studied over a frequency range from 40 Hz to 110 MHz as a function of temperature: two relaxations (micro-Brownian motion and interfacial polarization at low frequency and counterion polarization at high frequency) were observed in the SIPN microgel whose charges mainly exist in the PAA domains, and one relaxation (interfacial polarization) was observed in copolymer microgels whose charges distribute in the whole network, indicating that the structure of the charged microgel affects their relaxation behavior. The collapsing of the two microgels with different structures, PNIPAM/PAA SIPN and P(NIPAM-*co*-AA) microgels, was monitored near the VPTT with increase of temperature, and the electrical parameters of the collapsed microgels were calculated based on a model proposed for describing the dielectric properties of the microgel suspension. The results show that the VPTT of the microgels with different structures is different and in the following order: $VPTT_{P(NIPAM\text{-}co\text{-}AA)} > VPTT_{PNIPAM/PAA} > VPTT_{PNIPAM}$.

Besides, the temperature dependence of collapse parameters (C), permittivity and water content of microgel (ε_p, f_w) shows that the SIPN microgel has better low-temperature swelling properties. This is because the carboxyl group in the microgels interacts with water molecules in different binding modes: in the SIPN microgel, the hydrophilic carboxyl in domains interacts with water by a hydrogen bond; while in copolymer microgels, the hydrophilic carboxyl mainly forms a hydrogen bond with the surrounding amide. In addition, the SIPN microgel also has better thermal responsiveness than copolymer microgels. This is because in the P(NIPAM-*co*-AA) microgel the electrostatic repulsion between charged groups directly hinders the collapse of the microgel network, while in the SIPN microgel, the electrostatic repulsion is mainly from PAA domains and independent of PNIPAM. This is also the main reason for the higher VPTT of the copolymer microgel. Finally, the difference in the activation energy of the interfacial relaxation process for the two microgel systems also indicates that different structures will lead to different electrical properties of microgels.

This work may provide a new insight into the collapse process micromechanism of the two microgels with different charge distributions, essentially different structures. Particularly, the dielectric analysis based on the dielectric model of the dispersion system demonstrates its advantages in the quest for in-depth information of microgels.

Acknowledgements

The authors would like to thank Prof. Guanghui Ma, Prof. Yuxia Wang and Dr. Enping Lai of the Institute of Process Engineering,

Chinese Academy of Science for supplying the samples used in this work. The financial support from the National Natural Scientific Foundation of China (No. 21173025, 21473012) is gratefully acknowledged.

References

1 H. Chen, J. Li and Y. Ding, *et al.*, *Macromolecules*, 2005, **38**, 4403–4408.
2 G. I. Makhatadze and P. L. Privalov, *Adv. Protein Chem.*, 1995, **47**, 307–425.
3 Y. Guan and Y. J. Zhang, *Soft Matter*, 2011, **7**, 6375–6384.
4 F. d. r. Hapiot, S. p. Menuel and E. Monflier, *ACS Catal.*, 2013, **3**, 1006–1010.
5 T.-a. Asoh, T. Kaneko and M. Matsusaki, *et al.*, *J. Controlled Release*, 2006, **110**, 387–394.
6 J. Li, H. Cong and L. Li, *et al.*, *ACS Appl. Mater. Interfaces*, 2014, **6**, 13677–13687.
7 K. J. Krzyminski, M. Jasionowski and A. Gutowska, *Polym. Int.*, 2008, **57**, 592–604.
8 L. Sperling and R. Hu, *Polymer Blends Handbook*, Springer, 2014, pp. 677–724.
9 L. H. Sperling, *100+ Years of Plastics. Leo Baekeland and Beyond*, American Chemical Society, 2011, ch. 5, vol. 1080, pp. 69–82.
10 Y. Ye, Y. Shangguan and Y. Song, *et al.*, *Polymer*, 2014, **55**, 2445–2454.
11 K. Kratz, T. Hellweg and W. Eimer, *Colloids Surf., A*, 2000, **170**, 137–149.
12 H. Feil, Y. H. Bae and J. Feijen, *et al.*, *Macromolecules*, 1993, **26**, 2496–2500.
13 E. Y. Kozhunova, E. E. Makhaeva and A. R. Khokhlov, *Polymer*, 2012, **53**, 2379–2384.
14 B. Zhang, H. Tang and P. Wu, *Polym. Chem.*, 2014, **5**, 5967–5977.
15 M. Yang and K. Zhao, *J. Phys. Chem. B*, 2015, **119**, 13198–13207.
16 T. Hanai, *Kolloid-Z.*, 1960, **171**, 23–31.
17 M. Füllbrandt, R. von Klitzing and A. Schönhals, *Soft Matter*, 2013, **9**, 4464–4471.
18 J. F. Zhou, J. J. Wei and T. Ngai, *et al.*, *Macromolecules*, 2012, **45**, 6158–6167.
19 W. Su, K. Zhao and J. Wei, *et al.*, *Soft Matter*, 2014, **10**, 8711–8723.
20 Y. S. Lipatov and T. T. Alekseeva, *Phase-separated interpenetrating polymer networks*, Springer, 2007.
21 T. Si, Y. Wang and W. Wei, *et al.*, *React. Funct. Polym.*, 2011, **71**, 728–735.
22 Y. Wang, J. Qin and Y. Wei, *et al.*, *Powder Technol.*, 2013, **236**, 107–113.
23 E. Lai, Y. Wang and Y. Wei, *et al.*, *J. Appl. Polym. Sci.*, 2016, **133**, 43343.
24 H. Schwan, *Determination of Biological Impendence*, Academic Press, New York, 1963, p. 323.
25 M. Wübbenhorst and J. v. Turnhout, *Dielectrics Newsletter*, 2000.
26 A. Serghei, M. Tress and J. Sangoro, *et al.*, *Phys. Rev. B: Condens. Matter Mater. Phys.*, 2009, **80**, 184301.
27 S. Havriliak and S. Negami, *Polymer*, 1967, **8**, 161–205.
28 C. Grosse and K. R. Foster, *J. Phys. Chem.*, 1987, **91**, 3073–3076.
29 A. Delgado, F. Arroyo and F. González-Caballero, *et al.*, *Colloids Surf., A*, 1998, **140**, 139–149.
30 V. Shilov and S. Dukhin, *Kolloidn. Zh.*, 1970, **32**, 293–300.
31 S. S. Dukhin, V. N. Shilov and J. Bikerman, *J. Electrochem. Soc.*, 1974, **121**, 154C.
32 S. Sun, J. Hu and H. Tang, *et al.*, *J. Phys. Chem. B*, 2010, **114**, 9761–9770.
33 S. Dukhin, *Adv. Colloid Interface Sci.*, 1995, **61**, 17–49.
34 D. R. Lide, *CRC handbook of chemistry and physics*, CRC press, 2004.
35 A. Schönhals and F. Kremer, *Broadband Dielectric Spectroscopy*, Springer, 2003.
36 K. Zhao, K. Asami and J. Lei, *Colloid Polym. Sci.*, 2002, **280**, 1038–1044.
37 J. Wang, K. Zhao and L. Zhang, *Rheol. Acta*, 2013, **52**, 115–125.
38 X. Fan and K. Zhao, *Soft Matter*, 2014, **10**, 3259–3270.
39 T. Mori, M. Nakashima and Y. Fukuda, *et al.*, *Langmuir*, 2006, **22**, 4336–4342.
40 Y. Chen, D. Ding and Z. Mao, *et al.*, *Biomacromolecules*, 2008, **9**, 2609–2614.
41 F. Ilmain, T. Tanaka and E. Kokufuta, *Nature*, 1991, **349**, 400–401.
42 S. Nayak and L. A. Lyon, *Angew. Chem., Int. Ed.*, 2005, **44**, 7686–7708 (*Angew. Chem.*, 2005, **7117**, 7862–7886).
43 M. Quesada-Pérez, J. A. Maroto-Centeno and J. Forcada, *et al.*, *Soft Matter*, 2011, **7**, 10536–10547.
44 H. Eyring, *J. Chem. Phys.*, 1936, **4**, 283–291.
45 T. Blythe and D. Bloor, *Electrical Properties of Polymers*, Cambridge University Press, New York, 2005, pp. 66–69.

